

AD-A115 061

ALUMINUM CO OF AMERICA ALCOA CENTER PA ALCOA LABS
EVALUATION OF THE ENGINEERING PROPERTIES OF A COMMERCIALLY PROD—ETC(U)

N00019-79-C-0258

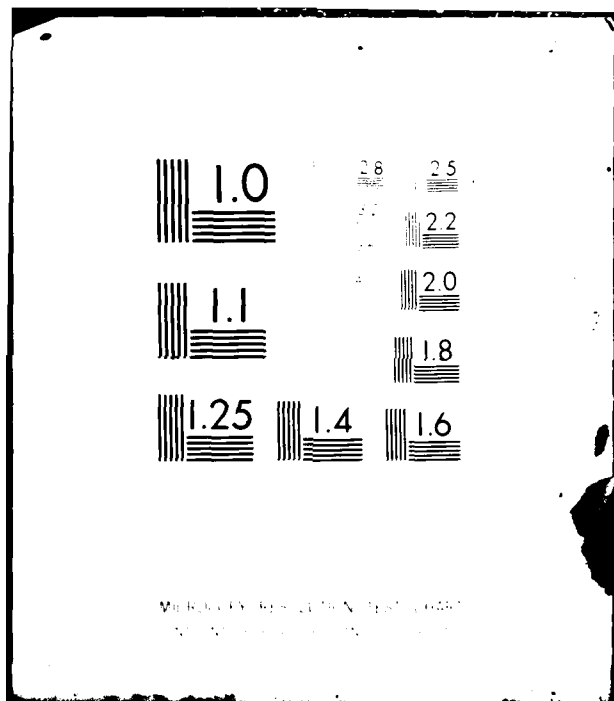
F/6 11/6

NL

UNCLASSIFIED

1 OF 1
AD-A
115-061

END
DATE
FILED
17-8-28
DTIC



McKee's Eye Clinic • 100 N. Main St., Galesburg
McKee's Eye Clinic • 100 N. Main St., Galesburg

Evaluation of the Engineering Properties of A C4000S-A Specified Aluminum Alloy 2020-T651 Plate

ADA115661

R.C. Malcolm
A.K. Vasudevan
P.J. Black
P.E. Bretz



**Packet Submitted to Final Agreement Under
Amendment to Contract N00019-79-C-0203**

**REGIMENT OF
ARTILLERY OF THE NAVY.
THE SISTER'S CONTINENT**

APPROVED FOR PUBLIC RELEASE
DISTRIBUTION UNLIMITED

NOTIC FILE COPY

TABLE OF CONTENTS

	<u>Page No.</u>
DD Form 1473	i
Foreword	ii
List of Tables	iii
List of Figures	iv-v
INTRODUCTION	1
OBJECTIVES	1
MATERIAL	2
SPECIMENS AND TEST PROCEDURES	2
1. Tensile Tests	2
2. Tear Tests	2
3. Fracture Toughness Tests	2-4
4. Fatigue Crack Growth (da/dN) Tests	4
MECHANICAL PROPERTIES	5
1. Tensile	5
2. Tear	5
3. Fracture Toughness	5-6
4. Fatigue Crack Growth (da/dN)	6-7
5. Fractographic Examination of FCG Specimen	7
SUMMARY	8
REFERENCES	9

Accession For	
NTIS, GPO&I	
DTIC TAB	
Unannounced	
Justification.....	
By.....	
Distribution/	
Availability Codes	
Actual and/or	
Dist	Special
A1	



UNCLASSIFIED

SECURITY CLASSIFICATION OF THIS PAGE (When Data Entered)

DD FORM 1 JAN 73 1473 EDITION OF 1 NOV 68 IS OBSOLETE.

UNCLASSIFIED

SECURITY CLASSIFICATION OF THIS PAGE (When Data Entered)

UNCLASSIFIED

SECURITY CLASSIFICATION OF THIS PAGE(When Data Entered)

and high elastic modulus, they possess low density and the potential for higher resistance to fatigue. Consequently, current research has been directed toward increasing fracture toughness of Al-Li type alloys into a range acceptable for aircraft use.

This report summarizes tensile, fracture toughness and fatigue crack growth properties obtained from a commercially produced lot of aluminum alloy 2020-T651 plate. This characterization is intended to serve as a baseline for alloy development work directed at improving damage tolerant characteristics of Al-Li type alloys. The fracture toughness characterization includes plane-strain fracture toughness (K_{Ic}) values, crack growth resistance (R) curves, as well as results from fracture toughness indicator tests; namely, the Kahn-type tear test and the slow bend precrack charpy test. Obtained fatigue crack growth rates traverse the entire range from near-threshold values to the exceedingly high rates encountered as ΔK values approach the material toughness. Metallographic characterization of alloy 2020-T651 in addition to fractographic results from a fatigue crack growth test specimen are also included in this report.

UNCLASSIFIED

SECURITY CLASSIFICATION OF THIS PAGE(When Data Entered)

FOREWORD

To assist studies in the area of aluminum-lithium alloy development, Alcoa requested the Navy supply samples of commercially produced 2020-T651 plate for the purpose of developing baseline engineering data. In exchange for two pieces of 2020-T651 plate from the Navy's inventory, Alcoa agreed to characterize the plate and submit the test results at no cost to the Navy. This transaction was handled as an amendment to Navy Contract No. N00019-79-C-0258 which was concurrently under way during the period 1979 July 1 to 1981 June 30 at Alcoa Laboratories, Alcoa Center, Pennsylvania. Mr. M. D. Valentine was the Navy Contract Monitor. R. J. Bucci served as Alcoa project manager, with R. C. Malcolm, A. K. Vasudevan, and P. E. Bretz as the principal Alcoa engineer/scientists for the program. A selected fatigue crack growth test was subcontracted to Del Research Corporation, Hellertown, Pennsylvania, under the direction of J. K. Donald and G. Miller as principal engineer.

LIST OF TABLES

<u>Table No.</u>		<u>Page No.</u>
1	Chemical Composition of Two (2) Pieces of Commercially Produced 32.54 mm (1.281-in.) Thick Aluminum Alloy 2020-T651 Plate	10
2	Results of Tensile Tests at Room Temperature of Two (2) Pieces of Commercially Produced 32.54 mm (1.281-in.) Thick Aluminum Alloy 2020-T651 Plate	11
3	Results of Tear Tests at Room Temperature of Two (2) Pieces of Commercially Produced 32.54 mm (1.281-in.) Thick Aluminum Alloy 2020-T651 Plate	12
4	Results of Fracture Toughness Tests (Plane-Strain (K_{Ic})), Slow-Bend Charpy (K_{ICh}) at Room Temperature of Two (2) Pieces of Commercially Produced 32.54 mm (1.281-in.) Thick Aluminum Alloy 2020-T651 Plate	13

LIST OF FIGURES

<u>Figure No.</u>		<u>Page No.</u>
1	Size and Shape of Two Pieces of Commercially Produced Alloy 2020-T651 (1.281-in. Thick) - Sample 523713 (A & B)	14
2	Photomicrograph Showing Grain Structure which is Typical of 2020-T651	15
3	Location of Test Specimens, Aluminum Alloy 2020-T651 Plate (Sample 523713, Piece A, Section 2)	16
4	Location of Test Specimens, Aluminum Alloy 2020-T651 Plate (Sample 523713, Piece B, Section 2)	17
5	Representative Tear Test Curve	18
6	R-Curve Toughness Data for Commercially Produced 2020-T651 Plate (32.54 mm Thick) in the Longitudinal (L-T) and Long-Transverse (T-L) Orientations	19
7	Slow-Bend Charpy Specimen	20
8	Slow Bend Charpy Test Set-Up	21
9	Representative Test Curve for Computer Logged Slow Bend Charpy Test	22
10	Effect of Specimen Orientation on the Fracture Path of Triplicate Kahn-Type Tear Specimens from a Sample (523713-A-2) of 2020-T651 Aluminum Alloy Plate (32.54 mm Thick)	23
11	Constant-Amplitude Fatigue Crack Propagation Data for Commercially Produced 2020-T651 Plate (32.54 mm Thick) in the Longitudinal (L-T) and Long-Transverse (T-L) Orientations (Moist Air Environment, R-Ratio = 0.33) . . .	24
12	Comparison of Constant-Amplitude Fatigue Crack Growth Rate Data Determined Using Visual Versus Compliance Methods of Crack Growth Measurement for Commercially Produced 2020-T651 Plate (32.54 mm Thick) in the Longitudinal (L-T) Orientation (Moist Air Environment, R-Ratio = 0.33) . . .	25

LIST OF FIGURES (continued)

<u>Figure No.</u>		<u>Page No.</u>
13	Comparison of the Constant-Amplitude Fatigue Crack Propagation Data for Samples of Commercially Produced 2020-T651 Plate (Moist Air Environment, R-Ratio = 0.33, L-T Orientation)	26
14	Comparison of Constant-Load-Amplitude Fatigue Crack Propagation Data for Commercially Produced 2020-T651 Plate with Data for Commercially and Laboratory Produced 7075-T651 Plate and Commercially Produced 7075-T7351 Plate (Moist Air Environment, R-Ratio = 0.33, L-T Orientation)	27
15(a&b)	Fracture Surface Appearance of Alloy 2020-T651 Plate (32.54 mm Thick) in the L-T Orientation for FCI Rates (da/dN) of 1.27×10^{-10} and 2.54×10^{-10} m/cycle (5×10^{-9} and 1×10^{-8} in./cycle, respectively)	28
15(c&d)	Fracture Surface Appearance of Alloy 2020-T651 Plate (32.54 mm Thick) in the L-T Orientation for FCI Rates (da/dN) of 1.27×10^{-9} and 1.27×10^{-8} m/cycle (5×10^{-8} and 5×10^{-7} in./cycle, respectively)	29
15(e&f)	Fracture Surface Appearance of Alloy 2020-T651 Plate (32.54 mm Thick) in the L-T Orientation for FCI Rates (da/dN) of 1.27×10^{-7} and 1.27×10^{-6} m/cycle (5×10^{-7} and 5×10^{-5} in./cycle, respectively)	30

EVALUATION OF THE ENGINEERING PROPERTIES OF A COMMERCIALLY
PRODUCED ALUMINUM ALLOY 2020-T651 PLATE

INTRODUCTION

Aluminum alloy 2020, which has a nominal composition of 4.5% Copper, 1.1% Lithium, 0.5% Magnesium, 0.1% Manganese and the balance Aluminum (93.7%), was developed in the 1950's to help satisfy the need for alloys with high strength and high modulus of elasticity for use in aircraft structures. However, alloy 2020, particularly in the peak strength temper (T6), developed low fracture toughness compared to that of commercial 7XXX alloys. This characteristic coupled with manufacturing difficulties led to the withdrawal of alloy 2020 for use in commercial products. Despite this setback, aluminum alloys containing lithium remain attractive for aircraft applications because in addition to high strength and high modulus of elasticity, they possess low density and the potential for higher resistance to cyclic loading conditions.(1, 2) Consequently, current research has been directed toward increasing fracture toughness of Al-Li-type alloys into a range acceptable for aircraft use.(3, 4)

To aid studies in the area of Al-Li-type alloy improvement, Alcoa requested the Navy supply some 2020-T651 plate for the purpose of developing engineering characteristics of alloy 2020 as a baseline material. In exchange for two pieces of aluminum alloy 2020-T651 plate (fabricated from the same lot) supplied by the Naval Air Systems Command, Alcoa agreed to characterize the plate and submit the test results and evaluations at no additional cost to the Navy. This transaction (4) was handled as an amendment to Navy Contract No. N00019-79-C-0256, "Effect of Microstructure on 7XXX Aluminum Alloy Fatigue Crack Growth at Low Stress Intensity."

OBJECTIVES

The properties agreed upon to be evaluated on the 2020-T651 plate are as follows:

1. Characterize microstructure by light microscopy,
2. chemical analysis,
3. tensile,
4. tear,
5. fracture toughness,
6. fatigue crack growth in humid air at room temperature (low, intermediate, and high ΔK), and
7. fractography.

MATERIAL

Two pieces of a single lot of commercially produced 32.54 mm (1.281-in.) thick 2020-T651 plate was supplied by the Navy for testing and study. Both pieces of plate were identical in size and shape, as shown in Fig. 1. Also, as indicated in Fig. 1, the rolling direction (longitudinal) of each piece of plate is parallel to the longest dimension (4.44 m or 14 ft. 7 in.). An Alcoa Technical Center sample number (523713) was assigned to each piece of plate with one denoted "A" and the other "B". A typical optical micrograph of the alloy is shown in Fig. 2. The structure is composed of coarse recrystallized grains. The grain size along longitudinal direction is .380 μm .

The chemical composition of each piece of plate was determined and the remelt analysis of each is shown in Table 1.

SPECIMENS AND TEST PROCEDURES

Test specimens to determine the various mechanical properties of both pieces of 2020-T651 plate were taken from Section 2 location in each piece, as shown in Fig. 1. The location of each individual specimen taken from Section 2 of pieces "A" and "B" is shown in Figs. 3 and 4, respectively. All the mechanical properties were determined from tests at room temperature on specimens taken in both the longitudinal and long-transverse orientations with respect to the rolling direction of each piece of plate.

1. Tensile Tests

The tensile tests were conducted in accordance with the ASTM Standard Method B557 using nominally 12.7 mm (0.500-in.) diameter specimens. Tests were made of both plate pieces "A" and "B" and in both the longitudinal (L) and long-transverse (LT) directions.

2. Tear Tests

The tear tests were made using nominally 2.54 mm (0.100-in.) thick Kahn-type tear test specimens. Tests were made of both plate pieces "A" and "B" and in both the longitudinal (L-T) and long-transverse (T-L) orientations.

The energy required to initiate and propagate a crack in each specimen were both determined from measurements of the appropriate areas under autographic load-deformation curves of the types represented in Fig. 5. The unit-propagation energy, which is used as an index of tear resistance, was determined for each specimen by dividing the net area of the specimen into the energy to propagate the crack. The ratio of the tear strength (the maximum nominal combined direct-and-bending stress developed by the specimen) to the tensile-yield strength was determined for each specimen for use as an index of toughness.

3. Fracture Toughness Tests

A. K_{Ic}

The fracture toughness K_{Ic} tests were conducted in accordance with the ASTM Standard Method E399 using nominally 31.8 mm (1.250-in.) thick compact-tension fracture toughness specimens, $W = 63.5$ mm (2.500-in.) and $2H = 76.2$ mm (3.000-in.).

Tests were made of both 100-1051 plate pieces "A" and "B" and in both the longitudinal (L-T) and long-transverse (T-L) orientations.

B. R-Curve

R-curve tests to determine material toughness were conducted in accordance with ASTM Standard Method H37 using nominally 0.35 mm (0.013-in.) thick steel compact fracture (PCF) specimens of the geometry shown in Fig. 4. Tests were made on specimens taken only from plate piece "B" and in both the L-T and T-L orientations.

Each specimen was initially precracked to a crack length about five percent greater than that corresponding to the initial machined notch. All specimens were loaded to failure at a controlled rate of displacement of 0.54 mm (0.1-in.) per minute at the load frame. During the loading, crack opening displacement (COD) values were measured by a clip-on displacement gage mounted at the crack mouth. The R-curve was recorded by defining a series of secant offset lines emanating from the origin (zero load point) and intersecting the autographic load-displacement curve. The offset defined by the secant offset defines an effective plastic compliance, which can be correlated to an effective crack length (a_{eff}) through the standard compliance relationship. The a_{eff} value represents the sum of the initial crack length (a_0) and the incremental effective crack extension (Δa_{eff}), the latter being the sum of the actual crack growth (Δa) and the crack tip plastic zone size (Δp) at the applied load. The K_I values are calculated using a general form of the secant intersection of the load vs. Δa data for input parameters to the stress intensity factor expression for the compact specimen.

C. Slow Bend Charpy

Slow bend charpy (SBC) tests, another bending fracture toughness indicator, were made using specimens of the configuration shown in Fig. 7. Tests were made on specimens taken only from plate piece "B" and in both the L-T and T-L orientations. Two SBC specimen thicknesses, 0.35 mm (0.013-in.) and the standard 10 mm (0.393-in.), were tested. The SBC specimens were fatigue precracked in simple bending to a nominal 5.18 mm (0.135-in.) length beyond the machined notch tip. Each specimen was then loaded to failure as a simply supported beam, as shown in Fig. 8, with deflection of the beam under load measured by two linear variable differential transformers (LVDT's). The electronic load and displacement signals were processed by computer and plotted as indicated in Fig. 9. One of the curves shown in the figure represents the total energy absorbed by the specimen and is calculated as the area under the load-deformation diagram.

Work by Ronald(5) and Wyponik(6) conducted on high strength titanium and aluminum alloys respectively, showed good correlation between K_{Ic} and SBC (K_{Ich}) toughness values calculated according to the following expression:

$$K_{Ich} = \left[\frac{E}{\delta} \left(\frac{W}{A} \right) \right]^{1/2}$$

where: E = material of elasticity;

\overline{W} = total work done fracturing the specimen given by the plateau value of the energy curve, see Fig. 1.

A = the initial area of the uncracked specimen ligament

$$\mu = \frac{1}{2} \ln \left(\frac{A_0}{A} \right) = .33.$$

a. Fatigue Crack Growth at RT Tests

Constant-load-amplitude fatigue crack growth (FCG) tests were conducted over low, intermediate and high stress intensity (K) ranges on specimens from the "B" plate of the 1-1-T plate. Crack-growth rate data was obtained using the constant-rate-of-loading (CRL) specimen, $b = 1.0$ mm (.04 in.) and $W = 65.5$ mm (.017 in.), in the 1-T and T-T orientationals. Three RT tests were made, two at the Alcoa Technical Center (one test of each orientation) and one at Del Research, Beloitown, PA (using an 1-T oriented specimen). All the testing was performed on 377 servo-controlled hydraulically-actuated clamps + mechanical test machine at a stress ratio ($R = K_{min}/K_{max}$) equal to 1.0 and a test frequency of 10 Hertz. The test environment was high humidity relative humidity > 90%)-room temperature-isothermal by air.

The precracking of the specimens tested at the Alcoa Technical Center was conducted by a sequence of stepped-load reductions (R-ratio = 1.0) with increasing crack extension. Upon attaining the desired value of K_{init} , the precrack phase was terminated and then FCG rate measurements were made at an increased with crack extension under fixed amplitude loading. The means of crack growth measurement was visual.

The precracking of the specimen tested at Del Research was conducted at an R-ratio of 1.1 with visual crack growth measurement. Upon attaining the desired crack length, a , the test parameters were applied. A automated test system utilizing a computer for data acquisition and machine control was used to obtain the crack growth rate data. The crack length was monitored continuously by using the elastic compliance technique, enabling the stress intensity to be controlled according to the equation:

$$K = K_0 \exp \left[-\beta (a-a_0)^n \right]$$

(K_0 is the initial cyclic stress intensity corresponding to the initial crack length, a_0 ; "a" is the current crack length, and "n" is a constant with the dimensions of 1/length(Y)). The test (K-decreasing) was conducted using a value of -36.1 mm $^{-1}$ (-1.5 in. $^{-1}$) for the parameter β . Also, for comparison, a couple of crack length measurements were made visually during the test.

The test procedures strictly adhered to the ASTM Tentative Test Method for Constant-Load-Amplitude Fatigue Crack Growth Rates At low da/dN (mm/cycle), K_{cyc} , and the proposed ASTM Standard test practice for measurement of very slow crack rates ($da/dN < 10^{-3}$ m/cycle)(8).

MECHANICAL PROPERTIES

1. Tensile

The results of the tensile tests of both pieces (A and B) of 2020-T651 plate in the L and LT directions are shown in Table 3. Duplicate tests were conducted for each condition, with the exception that four tests were made of piece "A" in the LT direction.

In general, the tensile properties of plate pieces "A" and "B" are comparable. Also, the tensile and yield strengths of each plate in the L and LT directions are comparable. However, the elongation and reduction of area values for both pieces of plate in the L direction are significantly higher than corresponding LT direction values.

2. Tear

The results of the tear tests of both pieces (A and B) of 2020-T651 plate in the L-T and T-L orientations are shown in Table 3. Triplicate tests were conducted for each condition.

In general, the tear strengths, ratios of tear strength to tensile-yield strength, and unit propagation energy values shown in Table 3 for both pieces of plate (A and B) are quite low, therefore, indicating that the fracture toughness of the 2020-T651 plate may not be very high. However, in general, the properties are comparable to those of another sample of Alcoa produced 34.9 mm (1.375-in.) thick 2020-T651 plate tested previously (unpublished Alcoa data).

The tear properties of plate piece "A" are slightly higher than those of piece "B". All of the L-T oriented tear specimens from both plate pieces fractured diagonally, as shown in Fig. 1^c, whereas the fracture path of each of the T-L oriented specimens is normal. The tear properties in the L-T orientation of both pieces of plate are significantly higher than those properties in the T-L orientation.

3. Fracture Toughness

A. K_{Ic}

The results of the K_{Ic} tests of both pieces (A and B) of 2020-T651 plate in the L-T and T-L orientations are shown in Table 4. Duplicate tests were conducted for each condition.

The tests on specimens in the L-T orientation of both pieces of plate resulted in valid K_{Ic} values, however, none of the tests in the T-L orientation resulted in valid K_{Ic} values. On the other hand, the K_{Ic} values for the T-L orientation of both plate "A" tests and one plate "B" test are considered meaningful. These test results show that the fracture toughness of plate pieces "A" and "B" are equal, however, the values are rather low indicating poor toughness. In general, the properties are comparable to those of two samples of Alcoa commercially produced 34.9 mm (1.375-in.) thick 2020-T651 plate tested previously (unpublished Alcoa data).

B. R-Curves

R-curves were developed from tests of specimens taken in the L-T and T-L orientations and only from plate piece "B". The data are shown in Fig. 6. Each curve is composed of data established from duplicate tests which were very reproducible. Out of plane fractures occurred in both the L-T oriented specimens, however not with the T-L oriented specimens. The data points recorded in Fig. 6 represent only those values where the plane of crack growth remained normal (to within $\pm 5^\circ$) to the applied loading direction. For the higher toughness L-T orientation, out of plane fracture occurred at Δa_{eff} values which correspond approximately to the point of maximum test load.

C. Slow Bend Charpy

Slow bend charpy ("CB") tests were conducted on specimens taken in the L-T and T-L orientations and only from plate piece "B". Four tests were made on specimens in each orientation, two each of 10 mm (0.395-in.) and 6.35 mm (.250-in.) thick specimens. The results of these tests are shown in Table 4.

The K_{Ic} values determined from the 6.35 mm (.250-in.) thick specimens are higher (on the average about 12 percent in the L-T orientation and 7 percent in the T-L orientation) than those values determined from the standard 10 mm (0.395-in.) thick specimens. The K_{Ic} values shown in Table 4 for the L-T oriented specimens are significantly higher than those for the T-L oriented specimens. Also, the fracture path observed in all the CB specimens tested (L-T and T-L orientations) retained their original plane, thereby eliminating the confounding effect of out of plane fracture on test interpretation.

The $K_{Ic,h}$ values are comparable to the K_Q values (Table 4).

D. Fatigue crack growth (da/dN)

Constant-load-amplitude fatigue crack growth (FCG) da/dN tests were made only on specimens from the 2024-T651 plate piece "B". Two tests were conducted on CT specimens in the L-T orientation and one in the T-L orientation at an R-ratio of 0.33 in a moist-air environment. Crack growth measurements for two of the tests (specimen number 1 in the L-T orientation and number 1 in the T-L orientation) were determined visually and those for one test (specimen number 2 in the L-T orientation) were determined electronically (compliance method). The crack growth rate data, at low, intermediate and high stress intensities (ΔK) for the three tests are shown plotted together in Fig. 11.

Some of the data shown in Fig. 11 violate an ASTM E647 requirement that at a given number of cycles any two crack lengths differing by more than 0.25R, actually 1.57 mm (0.062-in.) for these two tests, is invalid. However, since the requirement is not violated by much, not more than 0.84 mm (0.033-in.) in any instance, and a significant amount of critical low ΔK data is involved, this data is included in Fig. 11 (represented by solid symbols). This decision is also substantiated by the fact that there is sufficient data that does not violate the requirement that is interspersed with the invalid data and is in good agreement indicating that the slight violation of the ASTM requirement can be tolerated in this instance.

For the given test conditions, crack growth rates in the T-T orientation are significantly lower than those in the L-L orientation, and the crack growth rates in the T-T orientation are significantly higher than those in the L-L orientation. However, the growth rates in the two orientations are generally constant in the T-T orientation, as shown in Fig. 1e.

A comparison of the constant-rate crack growth data obtained with visual crack length measurements and crack growth measurements made by electrical capacitance tomography is given in Fig. 1e. Although the crack length measurements were taken at a position slightly further ahead than the data obtained with the crack growth丈ment, it is considered that the data are in close agreement. This is due to the fact that the crack length is constant, hence different crack positions can be distributed in mutual relation.

A comparison of the crack growth data for the T-T-Ti plate in the L-L orientation, characterized in this report, with similar data from a sample of another alloy prepared by the T-T-Ti plate, having 1.07-mm thickness, were previously reported elsewhere and shown in Fig. 1f. These data are summarized below, for reference and brief comparison.

Comparison of the T-T-Ti plate with the Ti-10-5 plate in the L-L orientation, with similar rates of crack growth and crack growth mechanisms, T-T-Ti plate and correspondingly prepared T-T-Ti plate, tested previously (unpublished data of the author), is shown in Fig. 1g. The T-T-Ti plate prepared at a temperature of 1,070°C has a similar crack growth rate to the Ti-10-5 plate in the L-L orientation, two times faster than initially and one-half times greater if the T-T-Ti plate is heated to 1,070°C and cooled to 1,000°C. The T-T-Ti plate and Ti-10-5 plate represent the first realization of two new alloys, the Ti-10-5 and T-T-Ti. In this regard, and for other reasons, the T-T-Ti plate is unique. At low, intermediate and high crack rates, the T-T-Ti plate generally exhibits superior resistance to crack growth after the same cracklength period in the T-T-Si or T-T-Ti/Si plate.

5. Fracture mechanisms

Figure 1b shows typical features of the fracture surface topography of alloy T-T-Ti plate piece "b", section 1, measured in the L-L orientation, at crack growth rates from 1.37×10^{-7} to 1.1×10^{-5} m/cycle (5×10^{-7} to 5×10^{-5} in./cycle, respectively). For crack rates up to 1.37×10^{-7} m/cycle (5×10^{-7} in./cycle), crack growth occurs primarily by a transgranular, intercrystallite mechanism (Figs. 1b₁ to 1b₄). A surface cracking is evident at 1.37×10^{-7} and 1.37×10^{-6} m/cycle (5×10^{-7} and 5×10^{-6} in./cycle, respectively), as indicated by the latter C in Figs. 1b₂ and 1b₄. A transition in fracture mechanism occurs at growth rates of 1.37×10^{-6} and 1.1×10^{-5} m/cycle (5×10^{-6} and 5×10^{-5} in./cycle, respectively), as shown in Figs. 1b₅ and 1b₆, respectively, to a mixed mode, dimpled fatigue-like intergranular fracture path. Several specific fracture surface features are apparent at these higher growth rates, as shown in Figs. 1b₇ and 1b₈, including fine-scale void formation (detail 1), void nucleation or constituent particles (detail 2), and intergranular fracture (detail 3). This fracture morphology in Figs. 1b₇ and 1b₈ is similar to that reported in a previous investigation¹ of the intermediate and high crack rate regimes.

SUMMARY

The chemical composition and various mechanical properties have been determined along with microstructural and fractographic examinations of a 32.54 mm (1.281-in.) thick sample of commercially produced 2020-T651 plate, two pieces (A and B), supplied by the Department of the Navy. The results of the various tests and examinations of the material are shown as follows:

1. Chemical Composition - Table 1
2. Microstructure Examination - Figure 2
3. Tensile Properties - Table 2
4. Tear Properties - Table 3
5. Fracture Toughness - Table 4 (K_{Ic} and Slow Bend Charpy) and Figure 6 (R-Curve)
6. Fatigue Crack Growth (FCG) - Figures 11 through 14
7. Fractographic Examination of FCG Specimen - Figure 15 (a-f)

The composition of the plate is about nominal for 2020 and the tensile properties of plate pieces "A" and "B" are comparable.

The fracture toughness of the plate is rather poor compared to 7XXX alloys and is indicated by the poor tear resistance and low K_{Ic} , R-curve and slow bend charpy values. On the other hand, the resistance of the 2020-T651 plate to constant-load-amplitude fatigue crack growth (FCG) at an R-ratio of 0.33 in a moist air environment is quite good over the low, intermediate and high ΔK ranges, and generally superior to 7075 plate in the T651 and T7351 tempers under similar conditions.

- 6 -

REFERENCES

1. R. H. Shanks and R. J. Wilkins, "Aluminum-Lithium Alloys: Low Density and High Strength," Metall Progress, March 1973, pp. 33-37.
2. R. H. Shanks and J. T. Stanley, "Review of Fatigue and Fracture Behavior of High-Strength Aluminum Alloys," Fatigue and Microstructure, American Society of Metals, Inc., pp. 401-433.
3. R. H. Shanks, "Fatigue, Fracture, Structure, Mechanical and Other Properties of Aluminum-Lithium Alloys," final report, Naval Air Development Center, Warminster, PA, NAG-7-1-171.
4. Letter from Louis J. George, Manager of R&D Contracts, Alcoa Laboratories, to Mr. J. W. Hartman, Contracting Officer, Department of the Navy, Naval Air Systems Command, Warminster, PA, Contract No. NGA-7-1-1255, 14 May 1973.
5. C. M. F. Reward, J. A. Hall, and C. M. Pierce, "Usefulness of Pre-cracked Charpy Specimens for Charpy Toughness Determining Test of Titanium Alloys," Materials Processing, Volume 5, April 1973, pp. 313-318.
6. R. H. Shanks, unpublished Alcoa data, 1973.
7. A. Kusaka, J. J. Kihak, Jr., J. K. Donald, P. W. Schmidt, "Computer-Automated K-Feathering Test Technique for Low Rate Fatigue Crack Growth Testing," J. Testing and Evaluation JETVA, Volume 1, May 1973.
8. R. J. Bucci, "Development of a Proposed Standard Practice for Near-Threshold Fatigue Crack Growth Rate Measurement," ASTM STP 735, American Society for Testing and Materials, 1981, pp. 5-38.

TABLE 1

CHEMICAL COMPOSITION^(a) OF TWO (2) PIECES^(b) OF COMMERCIALLY
PRODUCED 32.54 mm (1.281-in.) THICK ALUMINUM ALLOY 2020-T651 PLATE^(c)

Plate Piece Identification	Element, %								
	Si	Fe	Cu	Mn	Zn	Tl	Li	Cd	Al
A	0.09	0.20	4.48	0.53	0.03	0.02	1.06	0.19	93.40
B	0.09	0.20	4.44	0.52	0.03	0.02	1.09	0.20	93.41
Average	0.09	0.20	4.46	0.52	0.03	0.02	1.08	0.20	93.40
Nominal	--	--	4.5	0.5	--	--	1.1	0.2	93.7

NOTES: (a) Remelt analysis.
(b) Fabricated from a single lot.
(c) Sample No. 523713 (Alcoa number).

TABLE 2

RESULTS OF TENSILE TESTS AT ROOM TEMPERATURE OF TWO (2) PIECES (a) OF COMMERCIALLY PRODUCED 32.54 mm (1.28-in.) THICK ALUMINUM ALLOY 2020-T651 PLATE (b)

Plate (c) (d) Piece (e)	Specimen Orientation (e)	Specimen No.	TS (f) MPa	YS (g) KSI	El. in 4D, (h) %	R of A, (i) %
A	L	1 (j)	545.5	79.1	516	74.8
		2	543.5	78.8	516	74.8
		Average	544.5	79.0	516	74.8
B	L	1 (j)	550.5	79.8	519.5	75.3
		2 (j)	550	79.8	519.5	75.3
		Average	550.2	79.8	519.5	75.3
A	LT	1 (j) (k)	521.5	75.6 (l)	516	74.8
		2 (k)	480 (l)	69.6 (l)	(m)	0.9
		3 (k)	533.5	77.4	514	74.5
		4	520.5	75.5	514	74.5
	LT	525.2 (n)	76.2 (n)	514.7 (n)	74.7 (n)	0.9
		Average	525.2 (n)	76.2 (n)	514.7 (n)	74.7 (n)
		1 (j) (k)	541	78.5	521.5	75.6
		2 (j) (k)	538.5	78.1	521.5	75.6
B	LT	Average	539.8	78.3	521.5	75.6
		Average	539.8	78.3	521.5	75.6

NOTES:

- (a) Fabricated from a single lot.
- (b) Sample No. 523713 (Alcoa number).
- (c) Specimens taken from Section 2 in each piece (refer to Fig. 1 for location of Section 2).
- (d) Refer to FIGS. 3 and 4 for location of test specimens in pieces A and B, respectively.
- (e) Test specimens taken in the longitudinal (L) and long-transverse (LT) direction of rolling and from the center (T/2) location through the plate thickness.
- (f) TS = Tensile Strength.
- (g) YS = Yield Strength (0.2 percent offset).
- (h) El. in 4D = Elongation in 4 times specimen diameter.
- (i) R of A = Reduction of Area.
- (j) Specimen fragmented at fracture.
- (k) Specimen failed outside middle third of gage length.
- (l) Value not included in the determination of average value.
- (m) Value not obtained (specimen failed before reaching 0.2 percent offset).
- (n) Value represents the average of three (3) tests.

TABLE 3

RESULTS OF TEAR TESTS AT ROOM TEMPERATURE OF TWO (2) PIECES^(a) OF COMMERCIALY PRODUCED 32.54 mm (1.281-in.) THICK ALUMINUM ALLOY 2020-TM51 PLATE(B)

Plate(c)(d) Piece Identification	Specimen Orientation(e)	Specimen No.	TS(f) MPa	TS(g) KSI	TS/Y/S(h) Ratio	K _U /m ²	UPE(i) In.-lb/in. ²
A	L-T	1	4.95	62.1	0.83	30.2 ^(j) (J)	17 ^(k) (J)
		2	45.1	65.4	0.87	28.6 ^(l) (J)	16.3 ^(l) (J)
		3	398	57.7	0.77	26.2 ^(m) (J)	15.0 ^(m) (J)
B	L-T	1	4.11	61.8	0.83	28.3	16.2
		2	4.21	61.1	0.82	28.6 ⁽ⁿ⁾ (J)	16.5 ⁽ⁿ⁾ (J)
		3	4095	58.7	0.79	23.4 ^(o) (J)	14.4 ^(o) (J)
Properties from Unpublished Alcoa Data(p)	Average	416	60.3	0.81	25.7	14.7	
	L-T	396	51.6	0.68	20.1	11.5	
A	T-L	1	571	39.3	0.52	8.7 ^(k) (J)	50 ^(k) (J)
		2	281	40.8	0.54	23.3 ^(k) (J)	13.3 ^(k) (J)
		3	267	38.7	0.51	18.8 ^(k) (J)	10.7 ^(k) (J)
B	T-L	1	250	39.6	0.53	16.9	9.7
		2	264	36.3	0.48	0.11 ⁽ⁿ⁾ (m)	0 ⁽ⁿ⁾ (m)
		3	269	38.6	0.51	0.01 ⁽ⁿ⁾ (m)	0 ⁽ⁿ⁾ (m)
Properties from Unpublished Alcoa Data(p)	Average	298	37.4	0.49	(o)	(o)	
	T-L	233	36.7	0.48	8.8	5.0	

NOTES:

(a) Fabricated from a single lot.
(b) Sample No. 523713 (Alcoa number).

(c) Specimens taken from Section 2 in each piece (refer to Fig. 1 for location of Section 2).
(d) Refer to Figs. 3 and 4 for location of test specimens in pieces A and B, respectively.

(e) Test specimens taken in the longitudinal (L-T) and long-transverse (T-L) direction of rolling, and from the center (T/2) location through the plate thickness.

(f) TS = Tear Strength.

(g) TS/Y/S = Tear Strength divided by Tensile Yield Strength.

(h) UPE = Unit Propagation Energy.

(i) UPE may be estimated and slightly high (rapid and diagonal fracture).

(j) Value included in the determination of average value.

(k) UPE may be estimated (rapid fracture).

(l) Energy may be near zero (cuto, not reliable).

(m) Value not included in the determination of an average value.

(n) UPE is estimated (rapid fracture).

(o) Not determined.

(p) Properties represent the results of tests of one (1) commercially produced sample of 34.9 mm (1.375-in.) thick 3020-TM51 plate (one test in each orientation).

TABLE 4
RESULTS OF FRACTURE TOUGHNESS TESTS (PLANE-STRAIN (K_{Ic})), SLOW-BEND CHARPY (K_{ICh})
AT ROOM TEMPERATURE OF TWO (2) PIECES (a) & (b) COMMERCIAL ALLOY 2024-T651 PLATE (b)
PRODUCED 32.54 mm (1.281-in.) THICK ALUMINUM ALLOY 2024-T651 PLATE (b)

Plate (c)(d) Identification	Specimen Orientation (e)	Specimen No.	K _{Ic} Tests			Slow-bend Charpy Tests		
			K_Q	$\frac{K_Q}{\text{ksi/in.}}$	Valid $K_{Ic}(J)$	Measured $K_{Ic}(J)$	Specimen No.	K_{ICh}
A	L-T	1	23.6	21.5	Yes	—	—	—
		2	23.5	21.4	Yes	—	—	—
		Average	23.6	21.5	Yes	—	—	—
	T-L	1	23.5	21.4	Yes	—	1(k)	18.4
		2	23.6	21.5	Yes	—	2(k)	20.9
		Average	23.6	21.5	Yes	—	—	19.0
Properties from Unpublished Alcoa Data (1)	L-T	23.7(1)	21.6(1)	—	—	—	—	—
		23.7(1)	21.6(1)	—	—	—	—	—
		Average	23.7(1)	21.6(1)	—	—	—	—
	T-L	1	19.2	17.5	No (f)	Yes (g)	Yes (g)	Yes (g)
		2	19.0	17.3	No (f)	Yes (g)	Yes (g)	Yes (g)
		Average	19.1	17.4	No	Yes	Yes	Yes
B	T-L	1	18.8(g)	17.1(g)	No (f)	Yes (f)	1(k)	15.6
		2	18.6	16.9	No (f)	Yes (f)	2(k)	15.5
		Average	18.6(h)	16.9(h)	No	Yes	Average	14.2
	Properties from Unpublished Alcoa Data (1)	19.1(1)	17.4(1)	Yes	—	—	3(1)	16.3
		19.1(1)	17.4(1)	Yes	—	—	4(1)	16.8
		Average	19.1(1)	17.4(1)	Yes	—	Average	15.3
		Average	19.1(1)	17.4(1)	Yes	—	—	14.6

NOTES: (a) Fabricated from a single lot.

(b) Sample No. 523713 (Alcoa number).

(c) Specimens taken from Section 2 in each piece (prior to H.P. 1 for longitudinal direction).

(d) Refer to FIGS. 3 and 4 for location of test specimens in plates A and B, respectively.

(e) Test specimens taken in the longitudinal (L-T) and long-transverse (T-L) directions of rolling and from the center (1/2) location through the plate thickness.

(f) Test is invalid due to the K_I being greater than 0.60 K_Q for the last step of fracture cracking (measured range is up to 0.70 K_Q).

(g) Value not included in the determination of average value.

(h) Value represents the result of one (1) test.

(1) Properties represent the results of tests of two (2) commercially produced and heat treated 34.9 mm (1.375-in.) thick 2024-T651 plate (a total of 5 tests in each orientation).

(1) For ASTM Method E393.

(1) Specimen 6.35 mm (0.250-in.) in thickness.

(1) Specimen 6.35 mm (0.250-in.) in thickness.

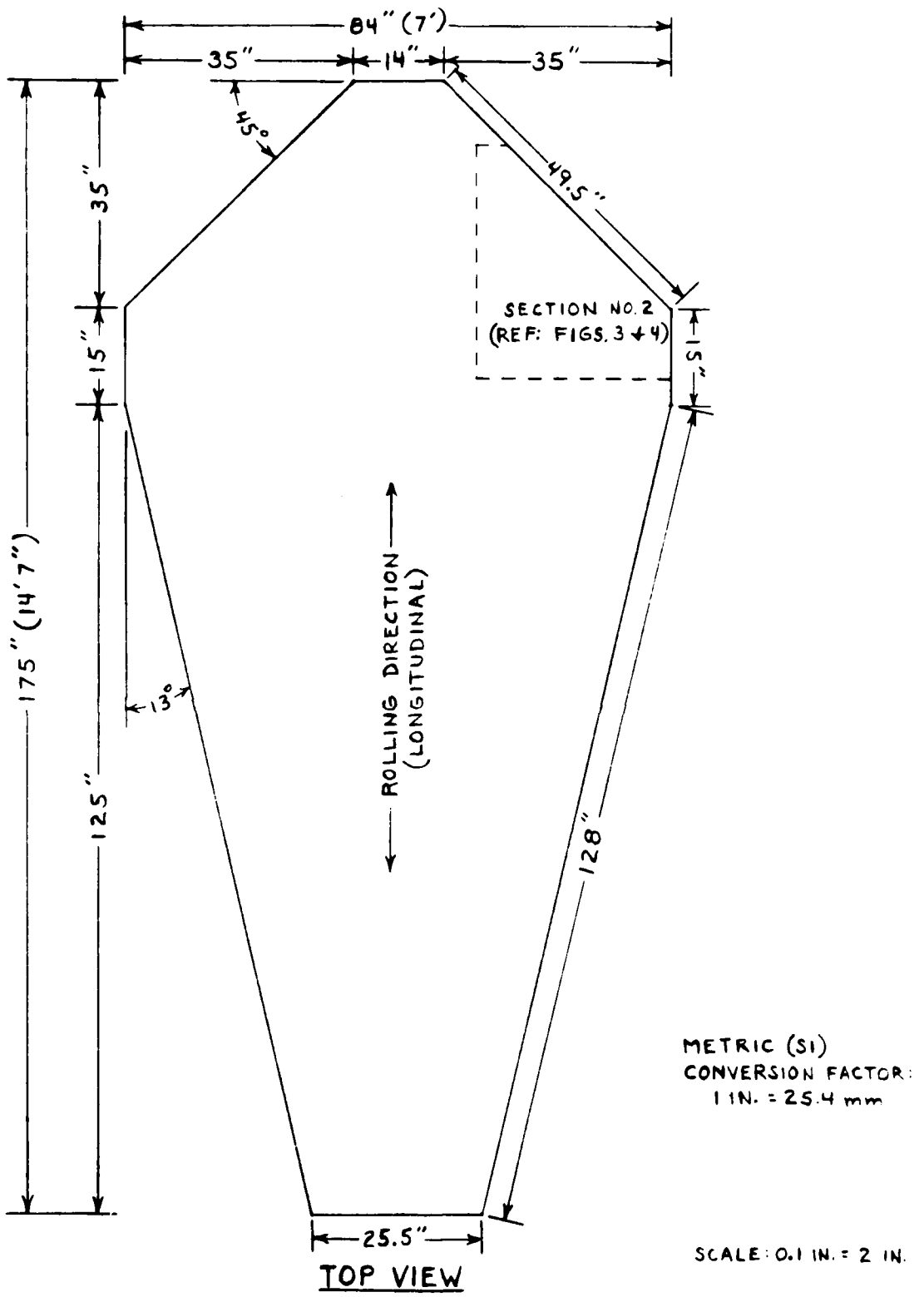
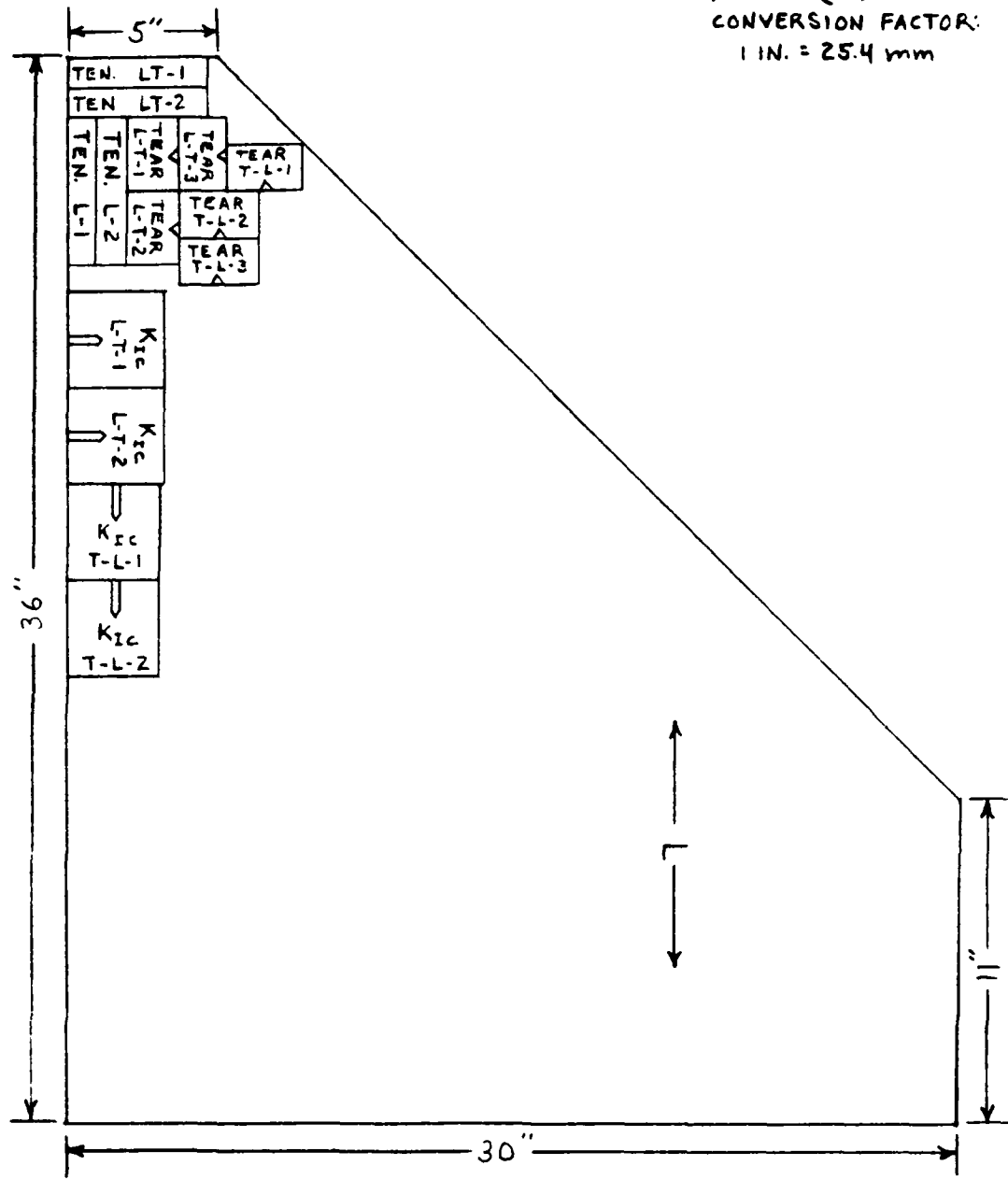


FIG. 1 SIZE AND SHAPE OF TWO PIECES OF COMMERCIALLY PRODUCED ALLOY 2020-T651 PLATE (1.281 IN. THICK) — SAMPLE 523713 (A+B)



METRIC (SI)
CONVERSION FACTOR:
1 IN. = 25.4 mm

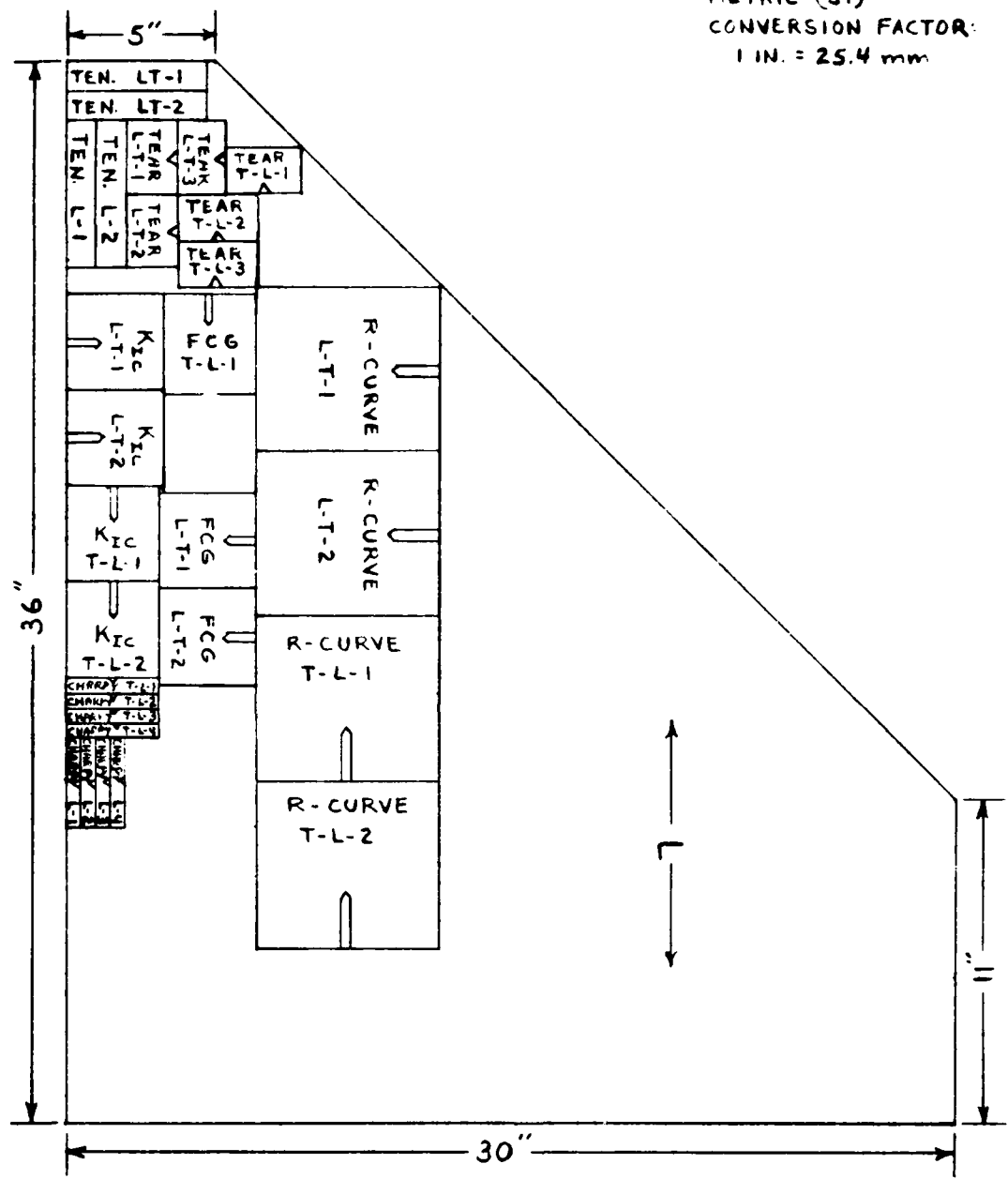


TOP VIEW

SCALE: 1 IN. = 5 IN.

FIG. 3 LOCATION OF TEST SPECIMENS, ALUMINUM ALLOY 2020-T651 PLATE
(SAMPLE 523713, PIECE A, SECTION 2)

METRIC (SI)
CONVERSION FACTOR:
1 IN. = 25.4 mm



TOP VIEW

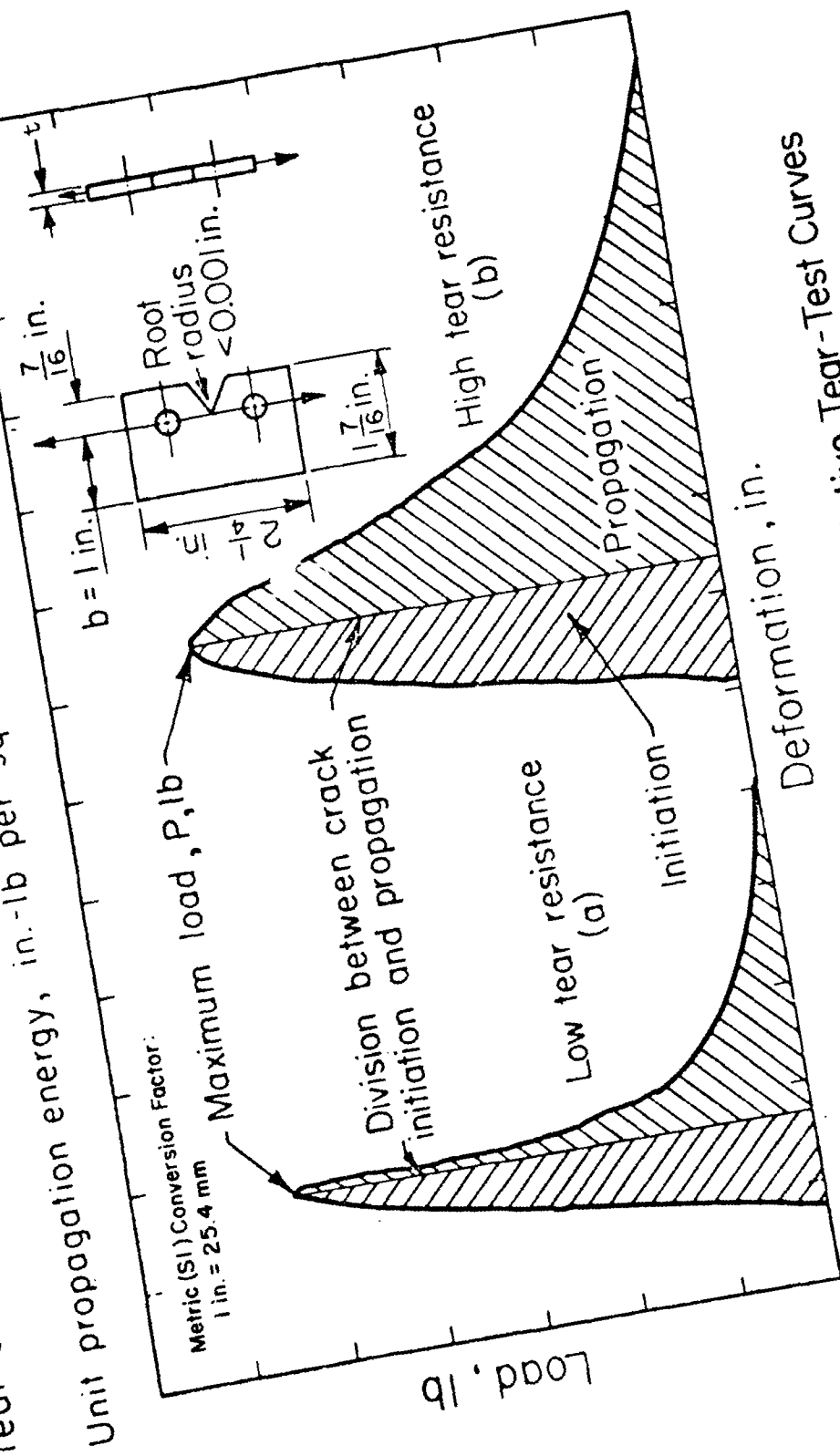
SCALE: 1 IN. = 5 IN.

FIG.4 LOCATION OF TEST SPECIMENS, ALUMINUM ALLOY 2020-T651 PLATE
(SAMPLE S23713, PIECE B, SECTION 2)

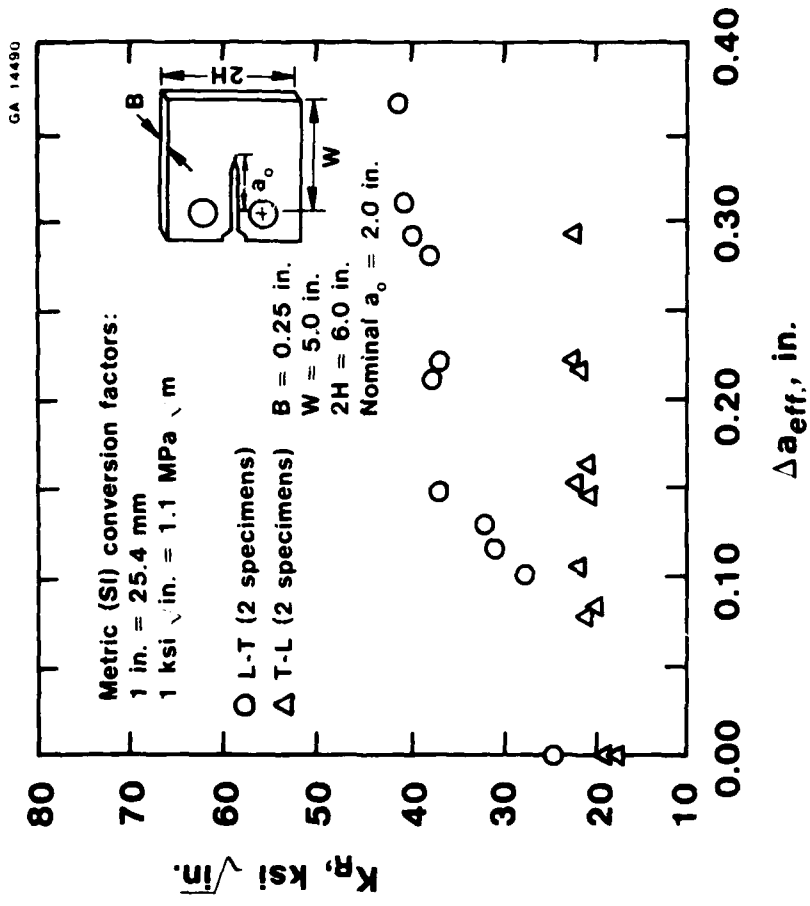
$$\text{Tear strength, psi} = \frac{P}{A} + \frac{MC}{I} = \frac{P}{bt} + \frac{3P}{bt} = \frac{4P}{bt}$$

energy to propagate a crack

$$\text{Unit propagation energy, in.-lb per sq in.} = \frac{\text{energy to propagate a crack}}{bt}$$

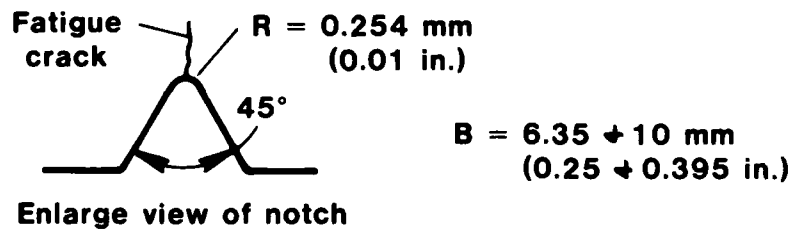
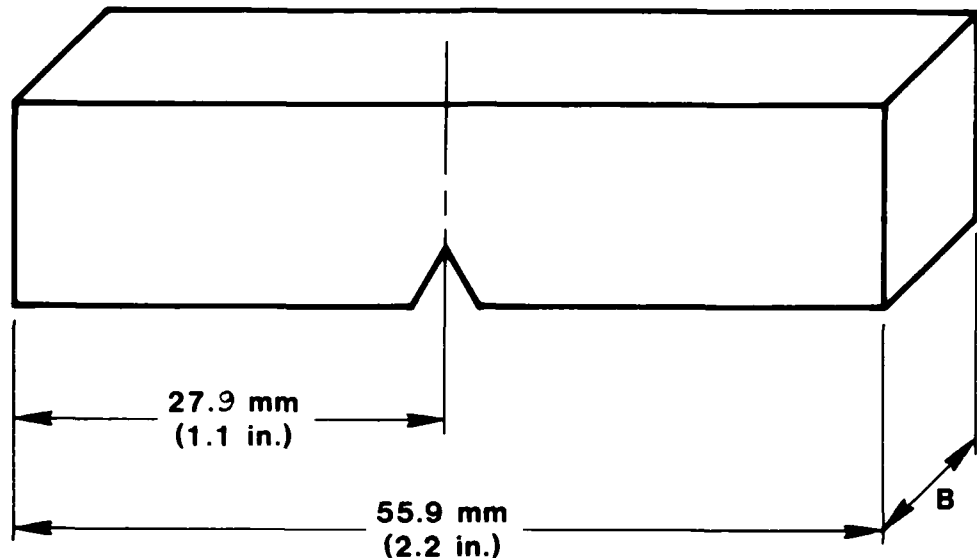


Tear-Test Specimen and Representative Tear-Test Curves
Figure 5

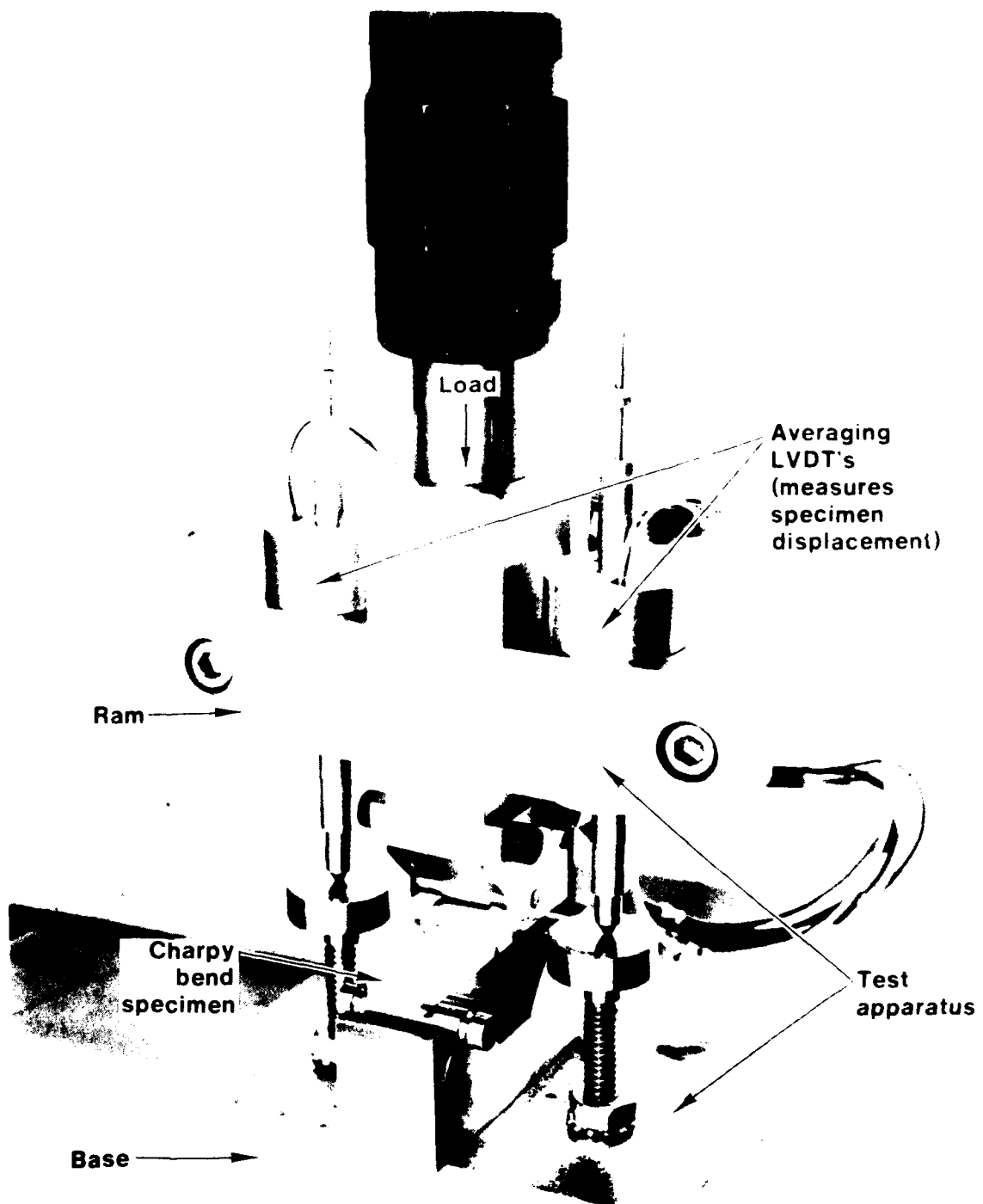


R-Curve Toughness Data for Commercially Produced 2020-T651 Plate (32.54 mm Thick) in the Longitudinal (L-T) and Long-Transverse (T-L) Orientations

Figure 6



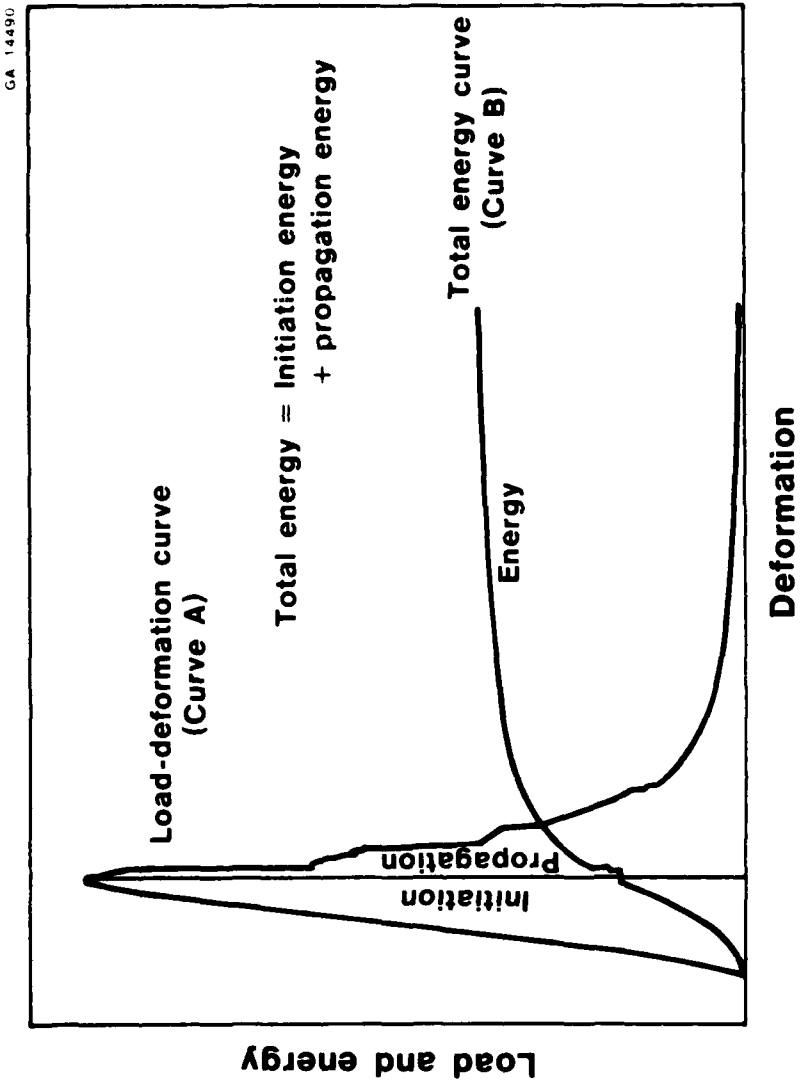
Slow-Bend Charpy Specimen
Figure 7

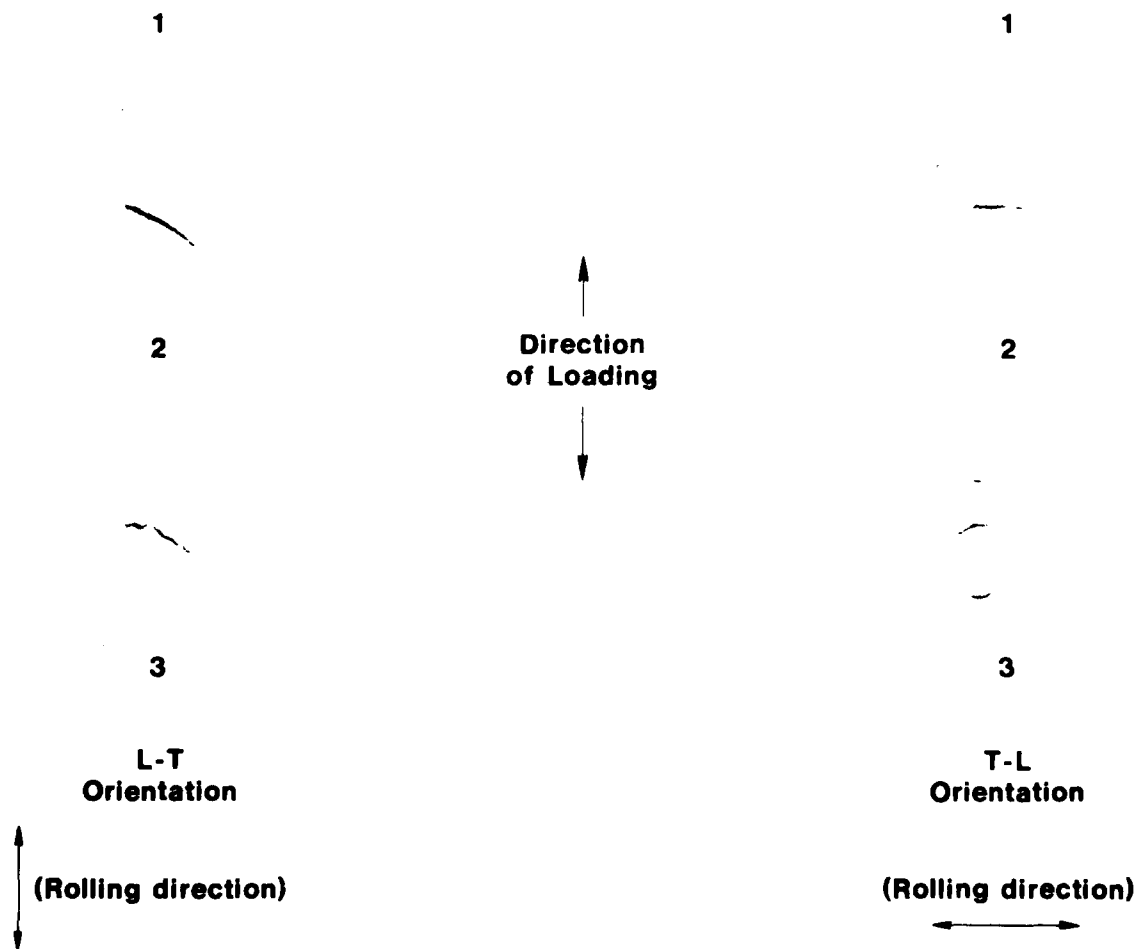


Slow-Bend Charpy Test Set-Up

Figure 8

Representative Test Curve for Computer Logged Slow-Bend Charpy Test
Figure 9





Effect of Specimen Orientation on the Fracture Path of Triplicate Kahn-Type Tear Specimens from a Sample (523713-A-2) of 2020-T651 Aluminum Alloy Plate (32.54 mm Thick)

Figure 10

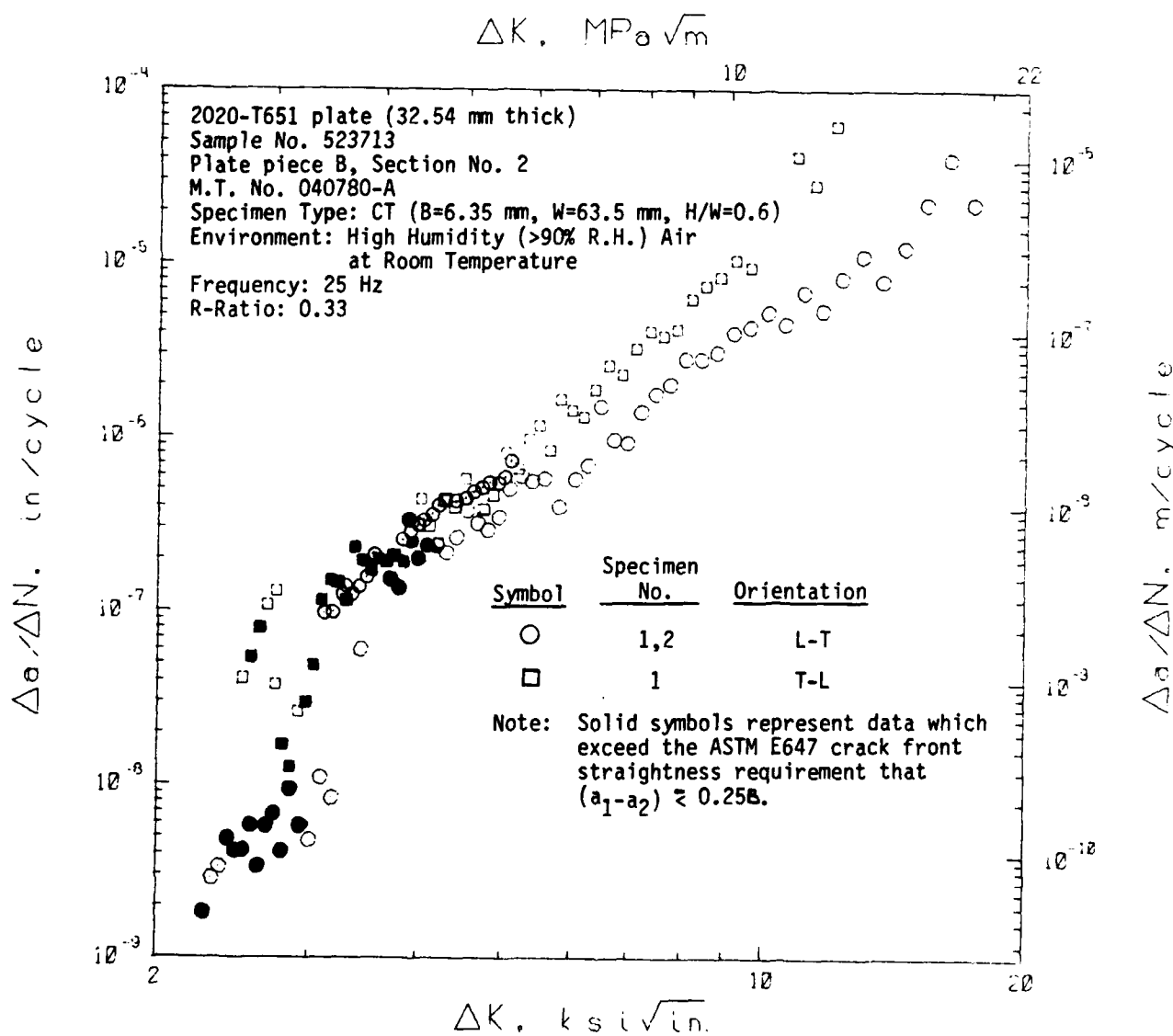


Fig. 11 Constant-Amplitude Fatigue Crack Propagation Data for Commercially Produced 2020-T651 Plate (32.54 mm thick) in the Longitudinal (L-T) and Long-Transverse (T-L) Orientations.
 (Moist Air Environment, R-Ratio=0.33)

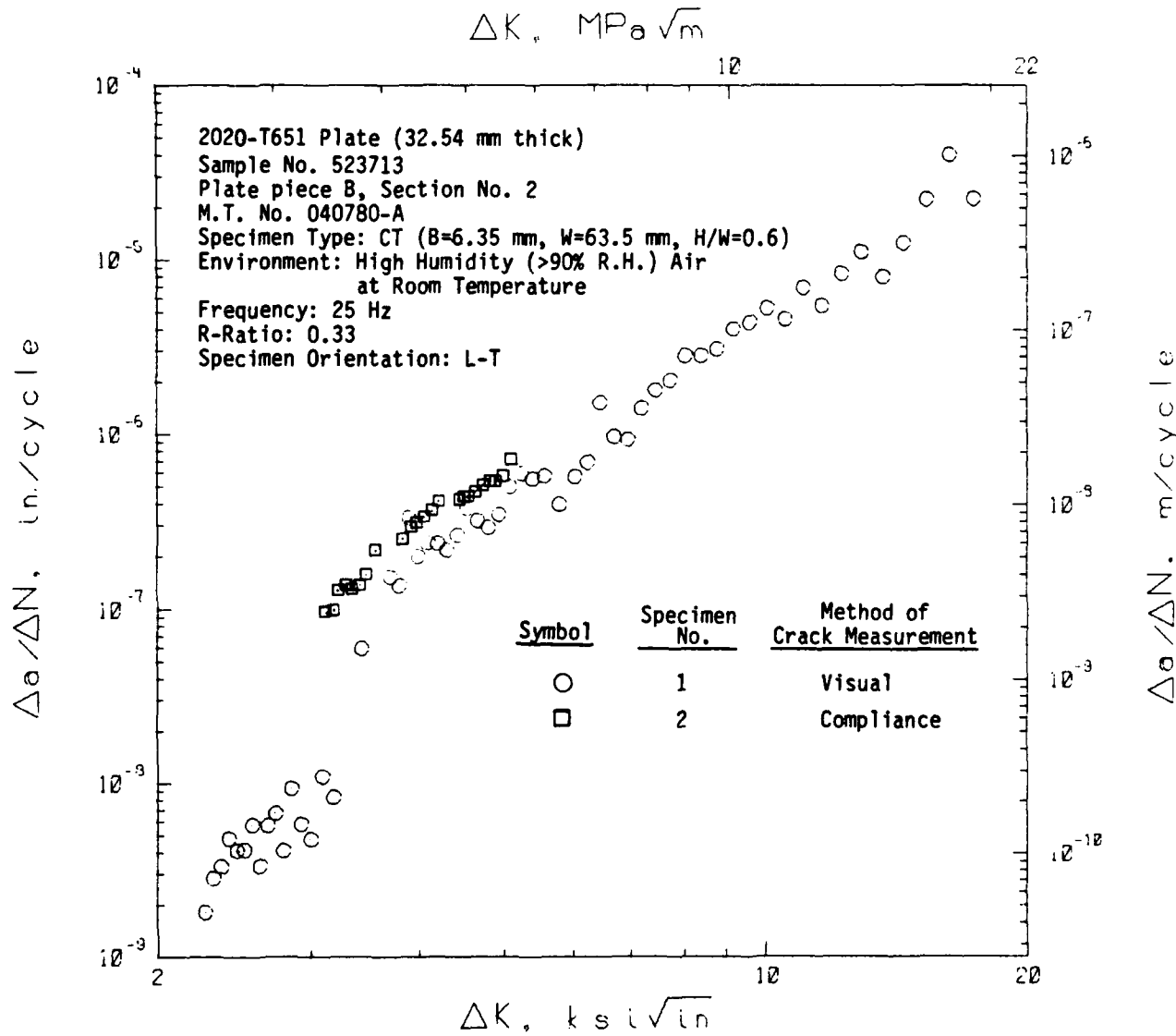


Fig. 12 Comparison of Constant-Amplitude Fatigue Crack Growth Rate Data Determined Using Visual Versus Compliance Methods of Crack Growth Measurement for Commercially Produced 2020-T651 Plate (32.54 mm thick) in the Longitudinal (L-T) Orientation
 (Moist Air Environment, R-Ratio=0.33)

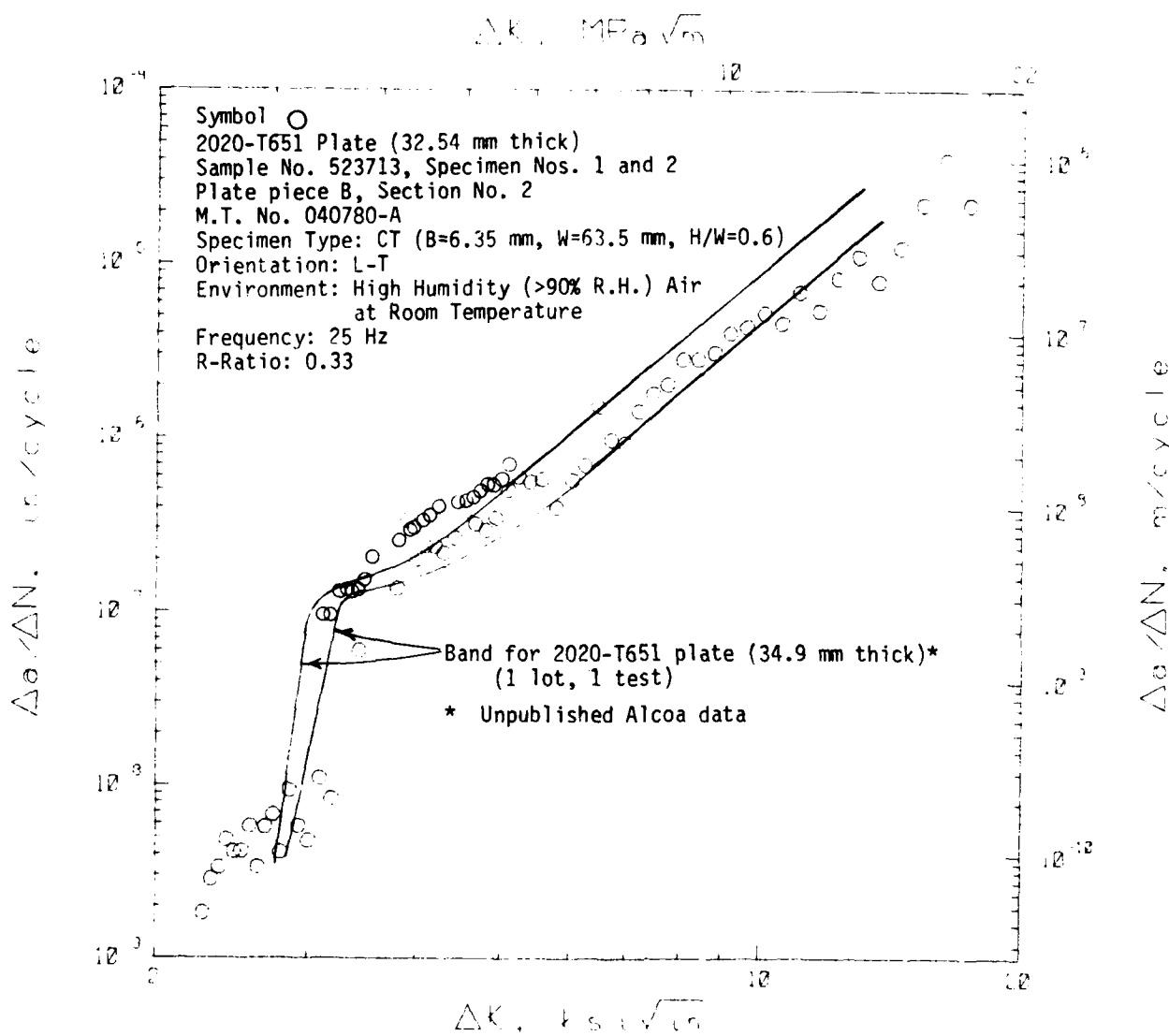


Fig. 13 Comparison of the Constant-Amplitude Fatigue Crack Propagation Data for Samples of Commercially Produced 2020-T651 Plate.
(Moist Air Environment, R-Ratio=0.33, L-T Orientation)

Symbol O
 2020-T651 Plate (22.54 mm thick)
 Sample No. 522713, Specimen Nos. 1 and 2
 Plate piece B, Section No. 2
 M.L. No. 040780-A
 Specimen Type: CT (B=6.35 mm, W=67.5 mm, H/W=0.6)
 Orientation: L-T
 Environment: High Humidity (>90% R.H.) Air
 at Room Temperature
 Frequency: 25 Hz
 R-Ratio: 0.33

Band for 7075-T651 Plate
 (2 commercially produced lots,* 3 tests⁴)
 1 laboratoryproduced lot,+ 3 tests
 * 6.35 and 76.2 mm thicknesses
 + 6.35 mm thickness

Band for 7075-T7351 Plate
 (2 commercially produced lots,* 3 tests⁴)
 * 25.4 and 34.9 mm thicknesses

⁴ Unpublished data
 + Ref. Navair Contract Nos.
 N00019-76-C-0482 and
 N00019-79-C-025R

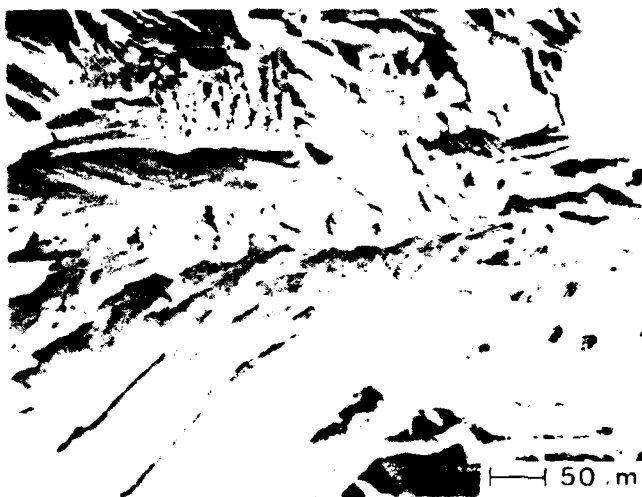
Fig. 14 Comparison of Constant-Load-Amplitude Fatigue Crack Propagation Data for Commercially Produced 2020-T651 Plate with Data for Commercially and Laboratory Produced 7075-T651 Plate and Commercially Produced 7075-T7351 Plate
 (Moist Air Environment, R-Ratio=0.33, L-T Orientation)

(a)
 $da/dN = 1.27 \times 10^{-10} \text{ m/cycle}$
 $(5 \times 10^{-9} \text{ in./cycle})$



Propagation direction

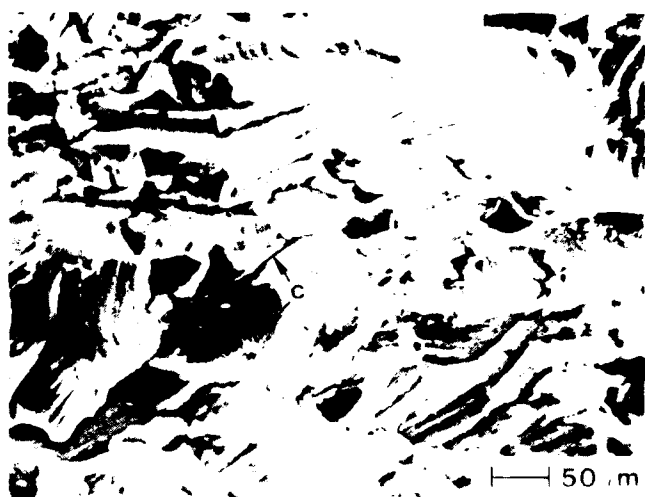
(b)
 $da/dN = 2.54 \times 10^{-10} \text{ m/cycle}$
 $(1 \times 10^{-8} \text{ in./cycle})$



**Fracture Surface Appearance of Alloy 2020-T651 Plate
(32.54 mm Thick) in the L-T Orientation for FCG Rates
(da/dN) of 1.27×10^{-10} and $2.54 \times 10^{-10} \text{ m/cycle}$
(5×10^{-9} and $1 \times 10^{-8} \text{ in./cycle}$, respectively)**

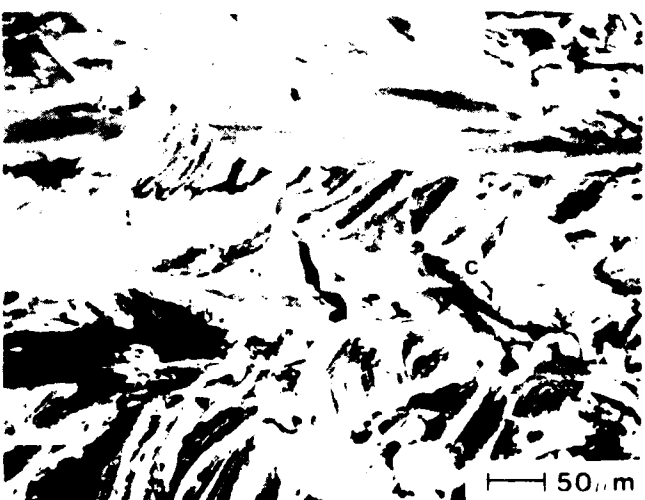
Figure 15 (a and b)

(c)
 $da/dN = 1.27 \times 10^{-9} \text{ m cycle}$
($5 \times 10^{-8} \text{ in. cycle}$)



Propagation direction

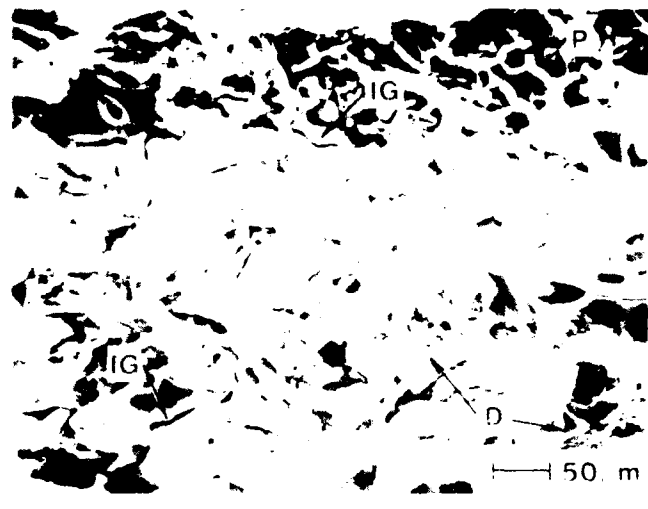
(d)
 $da/dN = 1.27 \times 10^{-8} \text{ m/cycle}$
($5 \times 10^{-7} \text{ in./cycle}$)



**Fracture Surface Appearance of Alloy 2020-T651 Plate
(32.54 mm Thick) in the L-T Orientation for FCG Rates
(da/dN) of 1.27×10^{-9} and $1.27 \times 10^{-8} \text{ m/cycle}$
(5×10^{-8} and $5 \times 10^{-7} \text{ in./cycle}$, respectively)**

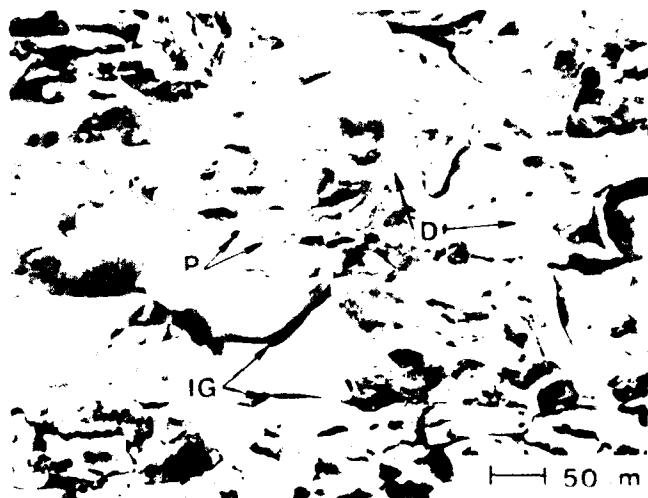
Figure 15 (c and d)

(e)
 $da/dN = 1.27 \times 10^{-7} \text{ m/cycle}$
($5 \times 10^{-6} \text{ in./cycle}$)



Propagation direction

(f)
 $da/dN = 1.27 \times 10^{-6} \text{ m/cycle}$
($5 \times 10^{-5} \text{ in./cycle}$)



**Fracture Surface Appearance of Alloy 2020-T651 Plate
(32.54 mm Thick) in the L-T Orientation for FCG Rates
(da/dN) of 1.27×10^{-7} and $1.27 \times 10^{-6} \text{ m/cycle}$
(5×10^{-6} and $5 \times 10^{-5} \text{ in./cycle}$, respectively)**

Figure 15 (e and f)

